Wall Inspection Control of a VTOL Unmanned Aerial Vehicle Based on a Stereo Optical Flow

Vincenzo Lippiello and Bruno Siciliano

Abstract— An autonomous wall inspection control based on a stereo optical flow, suitable for unmanned aerial vehicles endowed with a stereo vision system, is proposed in this paper. The inspection task consists of simultaneously controlling the inspection velocity along the surface, the relative yaw angle between the vehicle and the observed plane, as well as the orthogonal distance. A virtual spherical camera is considered at the center of gravity of the vehicle. Then, a stereo optical flow, as if it had been acquired by the virtual camera, is generated from the visual data provided by the stereo vision system. The 3D visual measurements are also employed to estimate the relative position and orientation of the observed plane. Hence, the absolute vehicle velocity is estimated by using a robust translational average optical flow by integrating the total stereo flow. Finally, an inspection control and a hovering control are proposed. The effectiveness of the described approach has been demonstrated with a dynamic simulation in an environment composed of two adjacent walls.

I. INTRODUCTION

In the last decade the scientific field of aerial robotics has generated a growing interest in the research community. Mainly due to the commercial potentialities of such technology, a number of new applications advance in the wide scenario of service robotics [1]. Some examples are remote sensing, disaster response, surveillance, inspection, search and rescue, communication, payload delivery, and image acquisition. Vertical takeoff and landing (VTOL) unmanned aerial vehicles (UAVs) are typically characterized by a limited payload and autonomy, as well as by small size and reduced cost. Moreover, highly coupled dynamics complicates the control problem for such systems, and thus the employment of nonlinear controllers and/or advanced sensing capabilities is often required.

Typically, an inertial measurement unit (IMU), which is composed of accelerometers and rate gyros, and a global positioning system (GPS) are available in standard UAV navigation systems. This latter is not effective in indoor and urban canyons environments and has not a sufficient bandwidth (1 Hz) for stabilization of a hovering vehicle. On the other hand, the angular velocity and the attitude can be estimated effectively with IMU data [2], while the

The authors are with PRISMA Lab, Dipartimento di Informatica e Sistemistica, Università degli Studi di Napoli Federico II, via Claudio 21, 80125, Naples, Italy vincenzo.lippiello@unina.it, bruno.siciliano@unina.it

translational position and the velocity can be estimated from low-cost IMU systems only for few seconds due to the growing of errors.

The adoption of on-board visual system is nowadays possible thanks to the use of ultralight and low-power consumption cameras and elaboration boards. Thanks to the use of such passive and adaptable sensors, along with IMU systems, a full-state estimation is possible by the adoption of suitable sensor fusion techniques [3], [4].

The estimation of the position and velocity can be avoided by using visual information directly for the design of the control law, namely a visual servoing control problem has to be considered [5], [6], [7]. Several control strategies have been inspired to the model of flying insects and are based on the visual flow [8], [9], [10]. Optical flow (OF) in the image space can be calculated in several ways [11], and can be used for docking manoeuvres [12], terrain-following [13], landing [14], obstacle avoidance [15], [16], and visual odometry [17]. Thanks to recent research achievements, several applications in unknown and cluttered environments, e.g. surveillance and inspection tasks, are now possible with an increasing reliability [18], [19], [20].

An autonomous wall inspection control, which employs the information provided by a stereo camera system to generate a virtual stereo OF, is proposed. The aim of this approach is the simultaneous control of the inspection velocity along the surface, of the orthogonal distance, and of the relative yaw angle between the UAV and the observed plane.

A virtual spherical camera is considered at the center of gravity (CoG) of the UAV. Thanks to an iterative algorithm, the camera is used to lead the acquisition process of the stereo pair generating both the stereo optical flow measurement, as if it had been really acquired by the virtual camera, and the estimation of the 3D planar surface parameters (orientation and relative distance). Then, an average translational OF is employed to estimate the absolute vehicle velocity. Finally, linear controllers are proposed for the execution of the wall inspection task, as well as for the hovering flight. The effectiveness of the proposed approach is shown with a simulation case study involving a virtual environment composed of two adjacent walls.

II. APPROACH OVERVIEW

The proposed visually-guided inspection algorithm is based on the virtualization of a spherical camera at the CoG of the UAV by employing the measurements provided by a stereo camera system. These measures are also employed
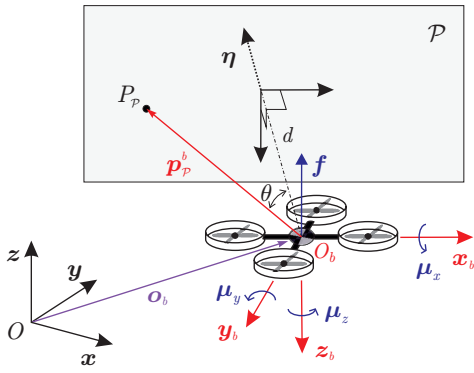
Fig. 1.   Reference frames and control inputs.

estimating the unknown orientation and the orthogonal distance of the observed surface with respect to the UAV. On the other hand, the virtual camera allows the definition of an OF useful for the estimation of the absolute vehicle velocity with respect to the observed surface in a very robust way. Based on these measurements, a navigation control for the autonomous inspection of a wall has been developed, which is able to separately control the planar velocity, the distance from the surface and the relative orientation.

In this paper some assumptions are made:

i)   the VTOL UAV is endowed with a calibrated stereo camera system;

ii)   the target surface is (locally) planar with a rich texture;

iii)   the points on the target surface are stationary in the inertial frame (i.e. the motion of the observed points depends only on the camera motion).

The paper is structured as follows. Section III provides the algorithm for the definition of the virtual spherical camera. The iterative procedure proposed for the target-plane parameters estimation is described in Section IV. Section V describes the image point kinematics, while the formulation of the average OF is proposed in Section VI. Section VII provides the dynamic model of the UAV employed for the control design. The proposed control laws, both for the inspection and the hovering tasks are described in Section VIII. Finally, a simulation case study is described in Section IX.

III. VIRTUAL SPHERICAL CAMERA

Let us consider an inertial reference frame $\mathcal{I} : \{O - \boldsymbol{xyz}\}$, which is fixed with respect to the earth surface, with the axis $\boldsymbol{z} = \begin{bmatrix} 0 & 0 & 1 \end{bmatrix}^{\mathrm{T}}$, and the body-fixed reference frame $\mathcal{B} : \{O_b - \boldsymbol{x}_b \boldsymbol{y}_b \boldsymbol{z}_b\}$, which is attached to the UAV at the CoG, as shown in Fig. 1. The position of the UAV with respect to the inertial frame is represented with the vector $\boldsymbol{o}_b = \begin{bmatrix} x & y & z \end{bmatrix}^{\mathrm{T}}$ and the orientation with the triplet of Euler roll-pitch-yaw angles $\boldsymbol{\phi} = (\varphi, \vartheta, \psi)$, i.e. with the rotation matrix $\boldsymbol{R}_b(\boldsymbol{\phi}) = \begin{bmatrix} \boldsymbol{x}_b & \boldsymbol{y}_b & \boldsymbol{z}_b \end{bmatrix} \in \mathrm{SO}(3)$ from $\mathcal{B}$ to $\mathcal{I}$. The linear and angular velocity of the vehicle with respect to $\mathcal{I}$ are represented by $\dot{\boldsymbol{p}}$ and $\boldsymbol{\omega}$, respectively.

The unit normal vector to the target plane $\mathcal{P}$ expressed in $\mathcal{I}$ is denoted with $\boldsymbol{\eta}$, while $d > 0$ denotes the orthogonal
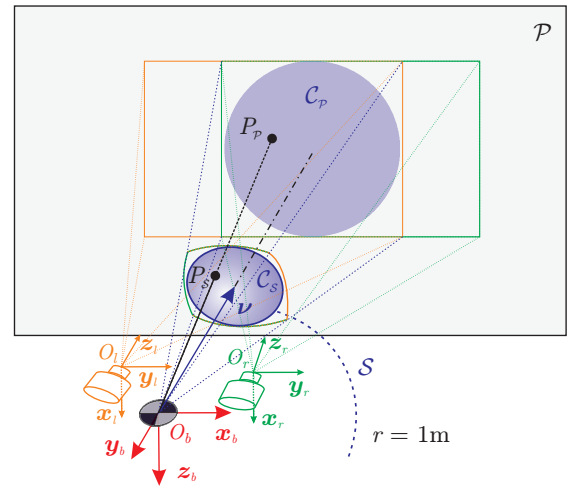
Fig. 2.   Stereo vision system and virtual spherical camera.

distance with respect to the the origin O_b of $\mathcal{B}$. Notice that the relative distance and orientation of the target plane with respect to $\mathcal{B}$ are univocally defined by $\boldsymbol{\eta}^b = \boldsymbol{R}_b^{\mathrm{T}} \boldsymbol{\eta}$ and d.

In order to exploit the passivity-like property addressed in [6], a virtual camera with a spherical image surface $\mathcal{S}$ with unit image radius (i.e. with unit focal length) is considered at the CoG of the UAV. With reference to Fig. 2, the projection of the fields of view of the available cameras onto the target plane generates a finite region of intersection that can be back-projected onto $\mathcal{S}$. Let $\mathcal{C}_{\mathcal{S}}(\boldsymbol{\nu}^b, \theta_{\mathcal{C}}) \subset \mathcal{S}$ denote the biggest spherical cap inside this back-projected surface, where $\boldsymbol{\nu}^b = \boldsymbol{R}_b^{\mathrm{T}} \boldsymbol{\nu}$ is the unit vector expressed in $\mathcal{B}$ pointing from O_b to the pole of the cap, and $\theta_{\mathcal{C}}$ is the the solid angle of the cap, which denotes the angle associated with the apex angle $2\theta_{\mathcal{C}}$. Notice that $\theta_{\mathcal{C}}$ depends both on the angles of view and on the image plane extensions of the stereo cameras, as well as on the relative orientation and distance of $\mathcal{P}$ with respect to the UAV.

The stereo vision system is composed of two cameras, namely the left and right cameras fixed with the reference frames $\mathcal{L} : \{O_l - \boldsymbol{x}_l \boldsymbol{y}_l \boldsymbol{z}_l\}$ and $\mathcal{R} : \{O_r - \boldsymbol{x}_r \boldsymbol{y}_r \boldsymbol{z}_r\}$, respectively, as shown in Fig. 2. Let $\boldsymbol{p}_{\mathcal{P}}^b$ denotes the position of a point $P_{\mathcal{P}} \in \mathcal{C}_{\mathcal{P}}$ with respect to $\mathcal{B}$, and let us consider the coordinates in pixel of its projections onto the image planes of both cameras $\boldsymbol{\sigma}_l = \begin{bmatrix} X_l & Y_l \end{bmatrix}^{\mathrm{T}}$ and $\boldsymbol{\sigma}_r = \begin{bmatrix} X_r & Y_r \end{bmatrix}^{\mathrm{T}}$, and their homogeneous representations $\tilde{\boldsymbol{\sigma}}_l = \begin{bmatrix} \boldsymbol{\sigma}_l^{\mathrm{T}} & 1 \end{bmatrix}^{\mathrm{T}}$ and $\tilde{\boldsymbol{\sigma}}_r = \begin{bmatrix} \boldsymbol{\sigma}_r^{\mathrm{T}} & 1 \end{bmatrix}^{\mathrm{T}}$. Hence, the normalized image coordinates $\boldsymbol{s}^l$ and $\boldsymbol{s}^r$, i.e. the projection onto the frontal image planes with unit focal lengths, can be evaluated as

$$\tilde{\boldsymbol{s}}_l = \boldsymbol{K}_l \tilde{\boldsymbol{\sigma}}^l \quad \text{and} \quad \tilde{\boldsymbol{s}}_r = \boldsymbol{K}_r \tilde{\boldsymbol{\sigma}}^r, \qquad (1)$$

respectively, where $\boldsymbol{K}_l$ and $\boldsymbol{K}_r$ are the cameras calibration matrices (i.e. the cameras intrinsic parameters).

By denoting with $\boldsymbol{o}_{bl}^b$ ($\boldsymbol{o}_{br}^b$) the position of the left (right) camera with respect to $\mathcal{B}$, and with $\boldsymbol{R}_l^b$ ($\boldsymbol{R}_r^b$) the corresponding rotation matrix (i.e. the cameras extrinsic parameters with

respect to $\mathcal{B}$), one can write

$$p_\mathcal{P}^b = o_{bl}^b + \lambda_l R_l^b s_l \qquad (2)$$

$$p_\mathcal{P}^b = o_{br}^b + \lambda_r R_r^b s_r, \qquad (3)$$

where a parametrical representation of the optical rays have been employed, with $\lambda_l > 0$ and $\lambda_r > 0$ unknown parameters. By combining (2) and (3), a system of 4 linear equations in p^b, with 3 unknowns, can be achieved. In the ideal case, the optical rays intersect in P and the equations are linearly dependent, while in the real case, due to image noise and optical distortions, the rays are often only close to intersecting and the equations are all independent. Several methods have been proposed to solve the matching and triangulation problem ensuring the minimization of some quality indices (e.g. by minimizing the image back-projection error) [21], [22], [23], [24].

Notice that the triangulation problem can be simplified if the stereo vision system is in the so-called *standard form*, e.g. with the optical axis perfectly aligned.

The projection of $P_\mathcal{P}$ onto the spherical surface $\mathcal{S}$ of the virtual camera, namely $P_\mathcal{S}$, can be retrieved by

$$p_\mathcal{S}^b = \frac{1}{\|p_\mathcal{P}^b\|} p_\mathcal{P}^b. \qquad (4)$$

IV. Target Plane Estimation

In this section, the iterative algorithm employed to estimate the pose of the target plane $\mathcal{P}$ on the basis of the visual measurements is described. An *acquisition grid* composed of N points uniformly distributed in $\mathcal{C}_\mathcal{S}$ is generated and projected onto the plane $\mathcal{P}$ (see Fig. 3), that has been estimated at the previous iteration. If required, this rough estimation of the current plane can be improved by using the previous measurement of the position and orientation of $\mathcal{P}$. This can be modified according to the (short-term) egomotion estimation of the UAV, i.e. the relative motion between two consecutive visual sampling times, that can be retrieved by integrating the linear acceleration and angular velocity measurements provided by the IMU [15].

Hence, the grid points are back projected onto the image planes of the stereo pair and are employed as points of interest for the matching and triangulation process. Let $\Pi_\mathcal{P}^b$ denote the $(N \times 3)$ matrix whose rows are the coordinates of the measured points with respect to $\mathcal{B}$, i.e.

$$\Pi_\mathcal{P}^b = \begin{bmatrix} p_{\mathcal{P}1}^b & \cdots & p_{\mathcal{P}N}^b \end{bmatrix}^\mathrm{T}. \qquad (5)$$

The singular value decomposition of $\Pi_\mathcal{P}^b$ is

$$\Pi_\mathcal{P}^b = V \Lambda V^\mathrm{T}, \qquad (6)$$

where $\Lambda = \mathrm{diag}\{\lambda_1, \lambda_2, \lambda_3\}$ is the diagonal matrix of the eigenvalues of $\Pi_\mathcal{P}^b$, and V is the (3×3) unitary matrix of the corresponding eigenvectors. Due to the quasi-planar distribution of the acquired points, which depends on the image measurement error, the smaller eigenvalue λ_3 is typically of one or two orders of magnitude less than the other ones (it is zero in the ideal case), and quantifies the spatial distribution of the measurement error along the orthogonal direction to
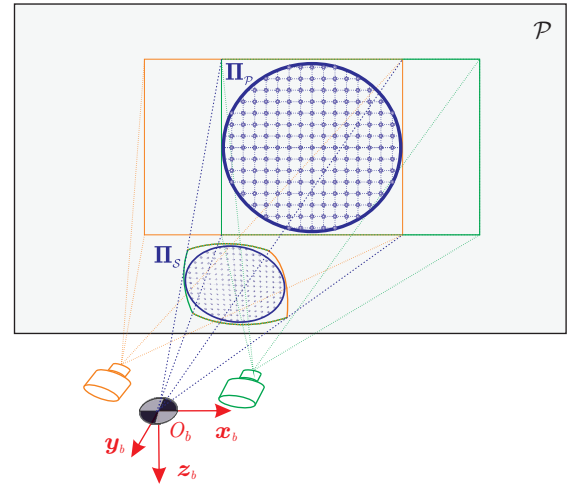
Fig. 3. Acquisition grid points.

$\mathcal{P}$ (i.e. η). Thus, the eigenvector associated to λ_3, i.e. the third column of V, is a useful measurement of η^b

$$\eta^b = V \begin{bmatrix} 0 \\ 0 \\ \gamma_\eta \end{bmatrix}, \qquad (7)$$

where $\gamma_\eta = \pm 1$ so as to achieve a unit vector pointing towards $\mathcal{P}$ with respect to the UAV.

The CoG of the measured points $\Pi_\mathcal{P}^b$ is considered to be a point laying on $\mathcal{P}$

$$b_\mathcal{P}^b = \frac{1}{N} \sum_{i=1}^N p_{\mathcal{P}i}^b. \qquad (8)$$

Hence, a measurement of the orthogonal distance of the UAV from the target plane is

$$d = \left(b_\mathcal{P}^b\right)^\mathrm{T} \eta^b, \qquad (9)$$

while a measure of the pole of $\mathcal{C}_\mathcal{P}$, i.e. of the principal optical axis ν, can be achieved as

$$\nu^b = \frac{1}{\|b_\mathcal{P}^b\|} b_\mathcal{P}^b. \qquad (10)$$

As initially described, these measurements and the IMU data are employed at the next iteration to roughly estimate the position and orientation of $\mathcal{P}$ at the current UAV position.

V. Image Point Kinematics

The motion of the image features on the virtual spherical camera, which is fixed with the UAV, is a function of the vehicle motion, being the plane fixed with respect to $\mathcal{I}$. The kinematics of the projection of an observed target point $p_\mathcal{P}^b \in \mathcal{P}$ onto the unit spherical surface $\mathcal{S}$ is inherited from the motion of the UAV (see [6], [25])

$$\dot{p}_\mathcal{S}^b = -\omega^b \times p_\mathcal{S}^b - \frac{1}{\|p_\mathcal{P}^b\|} N_p^b R_b^\mathrm{T} \dot{o}_b, \qquad (11)$$

where $\omega^b = R_b^\mathrm{T} \omega$, and $N_p^b = I_3 - p_\mathcal{S}^b (p_\mathcal{S}^b)^\mathrm{T}$ is a projector onto the tangent space of the sphere $\mathcal{S}$ at point $p_\mathcal{S}^b \in \mathcal{S}$, with I_3 the identity matrix.

By observing that for any target point $\boldsymbol{p}_{\mathcal{P}}^b \in \mathcal{P}$ one has

$$d = \left(\boldsymbol{p}_{\mathcal{P}}^b\right)^{\mathrm{T}} \boldsymbol{\eta}^b, \tag{12}$$

then combining (12) and (4) yields

$$\|\boldsymbol{p}_{\mathcal{P}}^b\| = \frac{d}{\left(\boldsymbol{p}_{\mathcal{S}}^b\right)^{\mathrm{T}} \boldsymbol{\eta}^b} = \frac{d}{\cos(\theta)}, \tag{13}$$

where θ is the angle between the normal direction to the target plane $\boldsymbol{\eta}$ and the observed target point. Substituting (13) into (11) yields

$$\dot{\boldsymbol{p}}_{\mathcal{S}}^b = -\boldsymbol{\omega}^b \times \boldsymbol{p}_{\mathcal{S}}^b - \frac{\cos(\theta)}{d} \boldsymbol{N}_p^b \boldsymbol{R}_b^{\mathrm{T}} \dot{\boldsymbol{o}}_b. \tag{14}$$

VI. AVERAGE OPTICAL FLOW

The rotational egomotion of the UAV, i.e. of the virtual spherical camera, produces both a translational and a rotational component in (14), as well described in [25]. When the observed surface is planar, the translational OF will have three components: the flow in the two planar directions, similar to classical OF, and the flow in the normal direction, analogous to optical divergence [13], [14]. As previously proposed in [7], an inertial translational OF from the integral of all the observed flow, corrected for rotational angular velocity, is considered for control purposes.

The translational OF can be obtained from the integral of the observed OF over the spherical cap $\mathcal{C}_{\mathcal{S}}$ around the pole pointed by $\boldsymbol{\nu}$, as shown in Fig. 2, that is given by

$$\boldsymbol{\phi} = \iint_{\mathcal{C}_{\mathcal{S}}} \dot{\boldsymbol{p}}_{\mathcal{S}}^b = -\pi(\sin\theta_{\mathcal{C}})^2 \boldsymbol{\omega}^b \times \boldsymbol{\nu}^b - \frac{1}{d} \boldsymbol{Q} \boldsymbol{R}_b^{\mathrm{T}} \dot{\boldsymbol{o}}_b, \tag{15}$$

where $\boldsymbol{\omega}^b$ is estimated from the IMU data [26], and $\boldsymbol{Q}$ is a symmetric positive definite matrix depending on the size of $\mathcal{C}_{\mathcal{S}}$ and on $\boldsymbol{\eta}$. In details, by denoting with (α_e, α_a) the spherical coordinates of $\boldsymbol{\nu}$, where α_e is the elevation angle and α_a is the azimuth angle, a rotation matrix with $\boldsymbol{\nu}$ in the z-axis assuming no rotation around $\boldsymbol{\nu}$ to the inertial frame $\mathcal{I}$ can be defined as

$$\boldsymbol{R}_\nu = \begin{bmatrix} c_{\alpha_e}c_{\alpha_a} & -s_{\alpha_a} & s_{\alpha_e}c_{\alpha_a} \\ c_{\alpha_e}s_{\alpha_a} & c_{\alpha_a} & s_{\alpha_e}s_{\alpha_a} \\ -s_{\alpha_e} & 0 & c_{\alpha_e} \end{bmatrix}, \tag{16}$$

where $c_x = \cos(x)$ and $s_x = \sin(x)$. Hence, $\boldsymbol{Q} = \boldsymbol{R}_b^{\mathrm{T}} \boldsymbol{R}_\nu \boldsymbol{\Lambda} \boldsymbol{R}_\nu^{\mathrm{T}} \boldsymbol{R}_b$, where $\boldsymbol{\Lambda}$ is a symmetric positive definite matrix, which can be evaluated as follows

$$\boldsymbol{\Lambda} = \iint_{\mathcal{C}_{\mathcal{S}}} (\boldsymbol{p}_{\mathcal{S}}^b)^{\mathrm{T}} \boldsymbol{\eta}^b \boldsymbol{N}_q^b d\boldsymbol{q}$$
$$= \int_{\theta=0}^{\theta_{\mathcal{C}}} \int_{\varphi=0}^{2\pi} \boldsymbol{q}^{\mathrm{T}} \boldsymbol{R}_\nu^{\mathrm{T}} \boldsymbol{\eta} (\boldsymbol{I} - \boldsymbol{q}\boldsymbol{q}^{\mathrm{T}}) \sin(\theta) d\theta d\varphi, \tag{17}$$

where $\boldsymbol{q} = \begin{bmatrix} s_\theta c_\varphi & s_\theta s_\varphi & c_\theta \end{bmatrix}^{\mathrm{T}}$. By solving (17), the following expression of $\boldsymbol{\Lambda}$ can be retrieved [13]

$$\boldsymbol{\Lambda} = \frac{\pi(\sin\theta_{\mathcal{C}})^4}{4} \begin{bmatrix} a/\lambda & 0 & b \\ 0 & a/\lambda & c \\ b & c & 2a \end{bmatrix}$$
$$a = c_{\beta_e}c_{\alpha_e} + s_{\beta_e}s_{\alpha_e}c_{\gamma_a}$$
$$b = c_{\beta_e}s_{\alpha_e} - s_{\beta_e}c_{\alpha_e}c_{\gamma_a} \tag{18}$$
$$c = -s_{\beta_e}s_{\alpha_e},$$

where (β_e, β_a) are the spherical coordinates of $\boldsymbol{\eta}$, $\gamma_e = \beta_e - \alpha_e$, and $\gamma_a = \beta_a - \alpha_a$. Notice that if $\boldsymbol{\eta} = \boldsymbol{\nu}$, i.e. if the UAV observes perpendicularly $\mathcal{P}$, then $\gamma_e = \gamma_a = 0$ and the matrix $\boldsymbol{\Lambda}$ becomes diagonal.

The average OF corrected for the angular velocity can be achieved from (15) as follows

$$\boldsymbol{w} = \frac{1}{d} \dot{\boldsymbol{o}}_b = -\boldsymbol{R}_\nu \boldsymbol{\Lambda}^{-1} \boldsymbol{R}_\nu^{\mathrm{T}} \boldsymbol{R}_b (\boldsymbol{\phi} + \pi(\sin\theta_{\mathcal{C}})^2 \boldsymbol{\omega}^b \times \boldsymbol{\nu}^b). \tag{19}$$

Thus, a measurement of the absolute vehicle velocity $\dot{\boldsymbol{o}}_b$ can be achieved from (19) by employing the orthogonal distance d, which has been measured as described in Section IV, and the average OF $\boldsymbol{w}$, which depends also on the measure of the orthogonal unit vector $\boldsymbol{\eta}$.

It is worth noticing that, when the value of $\theta_{\mathcal{C}}$ is limited (e.g. if wideangle cameras are not employed), the third component of $\boldsymbol{w}^b = \boldsymbol{R}_b^{\mathrm{T}} \boldsymbol{w}$, which acts analogously to OF divergence, is roughly estimated with respect to the first two components. On the other hand, if the baseline of the stereo pair is sufficient enough (e.g. not less than $10 \div 15$ cm), the orthogonal distance d is directly measured by the stereo vision system in (9) with good accuracy.

VII. VTOL UNDERACTUATED VEHICLE DYNAMICS

The VTOL UAV considered in this paper is modeled as a rigid body of mass m and tensor of inertia $\boldsymbol{J}$ and is supposed to be capable of a quasi-stationary flight. A translational force $\boldsymbol{f}$ combining thrust, lift and drag components, and a control torque $\boldsymbol{\mu}$ are applied to the vehicle by rotors. For quasi-stationary flight and a miniature vehicle, it is reasonable to assume $\boldsymbol{f}$ aligned with the axis $\boldsymbol{z}_b$ of $\mathcal{B}$, i.e. $\boldsymbol{f} = -\tau \boldsymbol{z}_b = -\tau \boldsymbol{R}_b \boldsymbol{z}$, where τ is a scalar input termed the thrust or heave, since the lift force is predominant with respect to the other components [27]. Hence, the dynamics of the UAV can be written as follows

$$m\ddot{\boldsymbol{o}}_b = -\tau \boldsymbol{R}_b \boldsymbol{z} - mg\boldsymbol{z} + \boldsymbol{\delta} \tag{20}$$
$$\boldsymbol{J}\dot{\boldsymbol{\omega}} = \boldsymbol{\mu} \tag{21}$$

where g is the gravity acceleration, and $\boldsymbol{\delta}$ represents unmodeled constant or slowly time-varying forces. By assuming that the orientation dynamics of the UAV are compensated with separate high-gain control loop, a hierarchical control can be considered for which a time scale separation exists between the translational dynamics (slow time scale) and the orientation dynamics (fast time scale).

By assuming to neglect the actuators dynamics, the desired value assigned to the thrust τ is instantaneously reached. Moreover, thanks to a high-gain controller, also the UAV orientation converges to the desired orientation $\boldsymbol{R}_b$. Hence, the control of the translational dynamics (20) with a vectorial control input $\boldsymbol{u} = \tau \boldsymbol{R}_b \boldsymbol{z}$ is mainly considered in this paper. Hence, the control problem is simplified as follows

$$m\ddot{\boldsymbol{o}}_b = -\boldsymbol{u} - mg\boldsymbol{z} + \boldsymbol{\delta}. \tag{22}$$

This approach is commonly employed in the practical solutions of the control problem, but nonetheless it can be theoretically justified using singular perturbation theory [28].

VIII. WALL INSPECTION CONTROL

The visually guided wall inspection task considered in this paper consists of three different subtasks that have to be simultaneously satisfied:

1) keep the principal optical axis $\boldsymbol{\nu}$ orthogonal to the wall;
2) hold a constant distance d from the wall;
3) follow a desired path in a plane parallel to the wall with a constant inspection velocity.

Moreover, hovering is also requested for the deep inspection of specific points of interest.

A. Optical axis control

The wall inspection Subtask 1) is required to ensure the best view angle required for the visual inspection of the wall and to maximize the area of the surface $\mathcal{C}_{\mathcal{P}} \in \mathcal{P}$ observed by the stereo pair. This subtask can be accomplished by assigning the desired value of the yaw angle to the low-level attitude control. In fact, the control input $\boldsymbol{u} = \tau \boldsymbol{R}_b(\boldsymbol{\phi})\boldsymbol{z}$ is composed of three components, while four degrees of freedom, namely τ and $\boldsymbol{\phi}$ are available. Hence, by reserving the $\boldsymbol{u}$ control input for Subtasks 2) and 3), the further degree of freedom can be employed to specify the desired yaw angle ψ_d so that the projection of $\boldsymbol{\nu}$ and $\boldsymbol{\eta}$ onto the xy-plane of $\mathcal{I}$ are coincident, or more precisely

$$\psi_d = \psi + \text{sgn}(\boldsymbol{z}^{\text{T}}(\boldsymbol{\nu}_{xy} \times \boldsymbol{\eta}_{xy})) \cos^{-1}\left(\frac{\boldsymbol{\nu}_{xy}^{\text{T}} \boldsymbol{\eta}_{xy}}{\|\boldsymbol{\nu}_{xy}\| \cdot \|\boldsymbol{\eta}_{xy}\|}\right), \tag{23}$$

where $\boldsymbol{v}_{xy} = \boldsymbol{v} - (\boldsymbol{v}^{\text{T}}\boldsymbol{z})\boldsymbol{z}$ is the projection of $\boldsymbol{v}$ onto the current xy-plane of the current reference frame, $\text{sgn}(\cdot)$ is the signum function, and the $\times$ operator indicates the cross product. Notice that the previous function is continuous with its derivative. Moreover, only if the wall is vertical, when the vehicle is hovering, then reaching of ψ_d leads to $\boldsymbol{\nu} = \boldsymbol{\eta}$.

B. Hovering control

Two different hovering control laws are here provided. First, the following PI control law with gravity compensation is proposed, that ensures the exponential stability of $\dot{\boldsymbol{o}}_b$

$$\boldsymbol{u}(t) = k_p d(t)\boldsymbol{w}(t) + k_i \int_0^t d(\tau)\boldsymbol{w}(\tau)\text{d}\tau - mg\boldsymbol{z}, \tag{24}$$

where k_p and k_i are positive parameters. In the following the dependence on time t is omitted for simplicity. By substituting (24) in (22), the dynamics of the closed-loop system becomes

$$m\ddot{\boldsymbol{o}}_b + k_p\dot{\boldsymbol{o}}_b + k_i(\boldsymbol{o}_b - \boldsymbol{o}_{b0}) = \boldsymbol{\delta}, \tag{25}$$

which ensures that $\boldsymbol{o}_b$ converges exponentially to $\boldsymbol{o}_{b0} + k_i^{-1}\boldsymbol{\delta}$. Moreover, in case of $\boldsymbol{\delta} = \boldsymbol{0}$ the position of the UAV stabilizes at its initial position.

However, in (24) the structural differences in terms of accuracy of the measured motion components are not fully exploited. Let us consider the rotation matrix $\boldsymbol{R}_{\mathcal{P}}$ of the target plane $\mathcal{P}$ with respect to $\mathcal{I}$, with $\boldsymbol{\eta}$ in the z-axis and

the y-axis aligned to the projection of $\boldsymbol{z}$ onto $\mathcal{P}$. With this change of coordinates, a new control input is considered

$$\boldsymbol{u} = \boldsymbol{R}_{\mathcal{P}}\boldsymbol{u}^{\mathcal{P}} - mg\boldsymbol{z}, \tag{26}$$

where $\boldsymbol{u}^{\mathcal{P}} \triangleq [\ \boldsymbol{u}^{\|\text{T}}\quad u^{\perp}\ ]^{\text{T}}$ is refered to $\mathcal{P}$ by means of its parallel and (scalar) orthogonal components. Notice how $u^{\perp}$ acts along the direction represented by $\boldsymbol{\eta}$ and is responsible for the dynamics of d, while $\boldsymbol{u}^{\|}$ has effect in a plane parallel to the wall and affects the performances of the inspection velocity control.

By multiplying both side of (22) for $\boldsymbol{R}_{\mathcal{P}}$ and substituting (26), the control problem can be rewritten in a partitioned form in $\mathcal{P}$ as follows

$$m\ddot{\boldsymbol{o}}_b^{\|} = -\boldsymbol{u}^{\|} + \boldsymbol{\delta}^{\|} \tag{27}$$
$$m\ddot{d} = -u^{\perp} + \delta^{\perp}, \tag{28}$$

where $\boldsymbol{R}_{\mathcal{P}}\ddot{\boldsymbol{o}}_b \triangleq [\ \ddot{\boldsymbol{o}}_b^{\|\text{T}}\quad \ddot{d}\ ]^{\text{T}}$ and $\boldsymbol{R}_{\mathcal{P}}\boldsymbol{\delta} \triangleq [\ \boldsymbol{\delta}^{\|\text{T}}\quad \delta^{\perp}\ ]^{\text{T}}$. Hence, the following control law is proposed

$$\boldsymbol{u}^{\|} = k_p^{\|} d\boldsymbol{w}_{xy} + k_i^{\|} \int_0^t d\boldsymbol{w}_{xy}\text{d}\tau \tag{29}$$

$$u^{\perp} = k_p^{\perp}(d - d_0) + k_d^{\perp} dw_z^{\mathcal{P}} + k_i^{\perp} \int_0^t (d - d_0)\text{d}\tau, \tag{30}$$

where $\boldsymbol{w}_{xy}^{\mathcal{P}}$ are the first two components and $w_z^{\mathcal{P}}$ is the third component of $\boldsymbol{R}_{\mathcal{P}}^{\text{T}}\boldsymbol{w}$, respectively, d_0 is the initial value of $d(t)$, and $k_p^{\|}$, $k_i^{\|}$, $k_p^{\perp}$, $k_d^{\perp}$, and $k_i^{\perp}$ are positive gain factors. In details, the control law (29) implements a PI controller on the measured parallel velocity, similarly to (24), while the control law (30) realizes a PID controller on the orthogonal distance error, with respect to the initial position, with the addition of a damping component proportional to the orthogonal velocity (notice that $\dot{d} = dw_z^{\mathcal{P}}$). It is straightforward to show that (29) stabilizes $\dot{\boldsymbol{o}}_b^{\|} = \boldsymbol{0}$, where $\dot{\boldsymbol{o}}_b^{\|}$ corresponds to the first two components of $\boldsymbol{R}_{\mathcal{P}}^{\text{T}}\dot{\boldsymbol{o}}_b$, and (30) ensures the exponential convergence of d to d_0 also in the presence of constant disturbances and unmodelled dynamics.

C. Inspection control

The control law (30) already guarantees the fulfilment of Subtask 2). Hence, a new expression for the control input $\boldsymbol{u}^{\|}$ has to be provided to ensure the achievement of Subtask 3). To this purpose, a PI controller on the parallel velocity error is proposed

$$\boldsymbol{u}^{\|} = \kappa_p^{\|}(d\boldsymbol{w}_{xy} - \dot{\boldsymbol{o}}_{b,d}^{\|}) + \kappa_i^{\|} \int_0^t (d\boldsymbol{w}_{xy} - \dot{\boldsymbol{o}}_{b,d}^{\|})d\tau, \tag{31}$$

where $\kappa_p^{\|} > 0$ and $\kappa_i^{\|} > 0$ are gain factors, and $\dot{\boldsymbol{o}}_{b,d}^{\|}$ is the constant desired velocity of the UAV in the plane parallel to $\mathcal{P}$, i.e. to the wall. With this control law, the closed-loop trajectory exists for all time, constant disturbances as well as unmodeled dynamics are rejected, and the velocity is exponentially stabilized to the desired value.
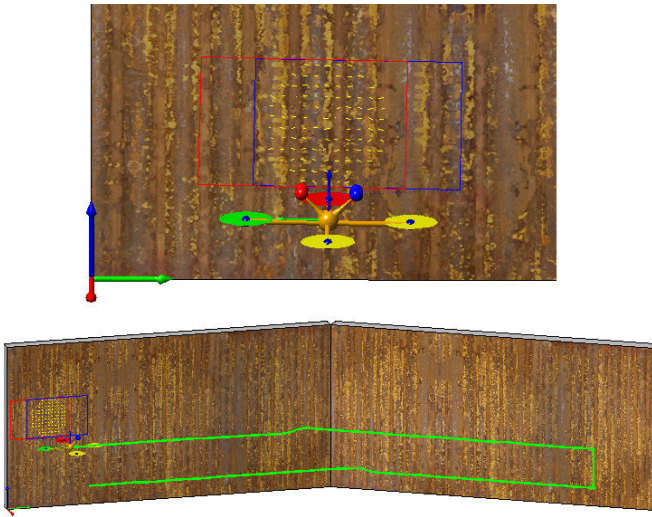
Fig. 4.   Simulation setup (top) and inspection path trajectory (bottom).

Fig. 5.   Time history of the yaw correction: desired (green) and executed (blue) trajectory. The vertical lines indicate the transition between the two planar surfaces.

Fig. 6.   Time history of the orthogonal distance with respect to the target planes: desired (green), estimated (red), and executed (blue) trajectory. The vertical lines indicate the transition between the two planar surfaces.

IX. SIMULATION RESULTS

A dynamic simulation of the proposed control framework has been performed by using the Matlab/Simulink environment. Figure 4 shows a sketch of the graphical animation of the UAV flying in front of a texturized wall (the texture corresponds to the photo of a real boiler wall), endowed with a stereo pair (the left and right cameras are shown in red and blue colors, respectively). The projection of the field of views of the cameras onto the wall, the measured grid points, as well as the corresponding measured OF are also shown.

The UAV is represented by a virtual point with a mass $m = 1.5$ kg and inertial matrix $\boldsymbol{J} = \mathrm{diag}(1e^{-2}, 1e^{-2}, 2e^{-2})$ kg m^2. The fast attitude inner-loop control produces a closed-loop system which is characterized by a second order dynamic system with a natural frequency of 7.5 Hz and a damping factor equal to 0.6.

The vision system is endowed with two identical cameras in a standard configuration, i.e. with the optical axes aligned, and with a baseline of 20 cm. A white Gaussian noise with a standard deviation of 2 mm is added to the measurements of the triangulated points of the acquisition grid to simulate the image noise. No outliers are considered. The visual system, as well as the control system, runs at 10 Hz.

The environment is composed of two adjacent (4×2) m planar surfaces rotated relatively to one other of 30 degrees.

The desired trajectory consists of two horizontal inspection rows (see Fig. 4), which have to be followed at a velocity of 25 cm/s with a constant orthogonal distance of 1 m, separated by an ascending trajectory to move from the horizontal paths. The final position is kept by the proposed hovering controller for 5 s. A supervisory control is employed to detect the reach of the end of the current surface, and then to switch from the constant-velocity inspection task to the ascending motion task, as well as to the hovering control mode.

The time history of the yaw angle correction generated by means of (23) is shown in Fig. 5. The vertical dotted lines indicate the time instant when the UAV travels from a target
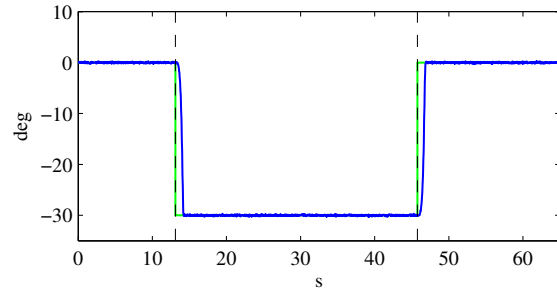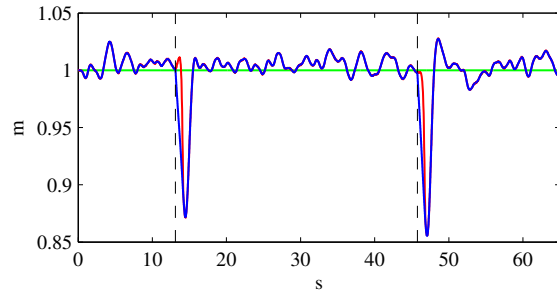
surface to the other one, with the consequent changing of the plane reference frame, which is employed for the generation of the desired reference values. During the transition of $\mathcal{C}_{\mathcal{P}}$ between the planes, the measurements of the plane parameters change smoothly to their right values. In fact, the discontinuities of the surfaces that the UAV meets along the way are completely absorbed by the integration of the OF operation, from one side, and by the average on all the grid points, from the other side. During the cruise trajectory, instead, the algorithm estimates the current plane parameters without any problem.

Figure 6 shows the estimated and the achieved orthogonal distance from the planes. Also in this case, the estimation of the distance of the plane change smoothly during the planes transition. However, it is noticeable how the transitions generate a significant relative estimation error of about 15%. This is partially due to the choice of the employed control gains, which have been chosen to achieve a settling time of $2 \div 3$ s and a damping factor equal to 0.75. Nevertheless, the executed trajectory, which has been achieved by employing the control law (30), follows the estimated one, i.e. the input reference, with a good accuracy and a limited overshoot.

Finally, the time history of the velocity estimation and of the true velocity are shown on Fig. 7 for both the parallel motion components (the y-component is aligned with the $\boldsymbol{z}$-axis of $\mathcal{I}$, i.e. with the gravity). It is important to notice how the absolute velocity is estimated with a good accuracy and without the presence of any scale factor. However, also in
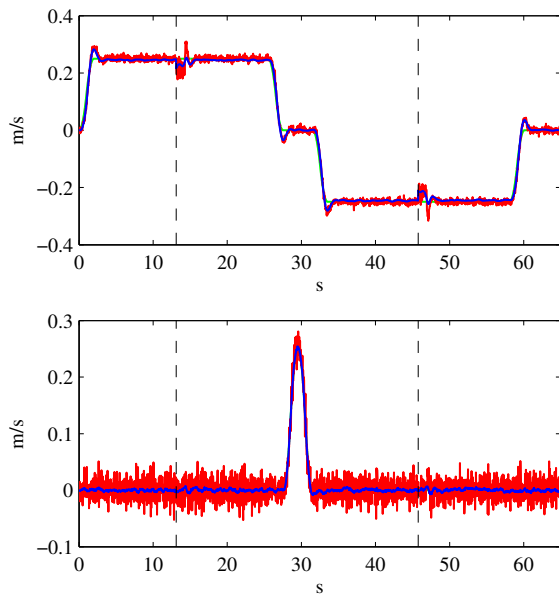
Fig. 7. Time history of the UAV velocity with respect to the target planes: desired (green), estimated (red), and executed (blue) trajectories. On the top (bottom) the trajectory of the $x(y)$-component is represented. The vertical lines indicate the transition between the two planar surfaces.

this case, the plane transitions generate a visible estimation error, that is quickly recovered when the discontinuity has been overcome and a planar region is again observed. In fact, the desired cruise velocity of 25 cm/s is guaranteed on both planes and also during the transition with a limited error.

X. CONCLUSION

An autonomous wall inspection control for UAVs based on a stereo optical flow has been proposed. A virtual spherical camera has been considered at the CoG of the vehicle. The visual stereo measurements have been used to generate a stereo optical flow and to estimate the 3D parameters of the observed plane. The absolute vehicle velocity has been estimated by using a translational average optical flow based on the reconstructed stereo optical flow. Finally, the proposed inspection control, as well as the hovering control, have been designed. The effectiveness of the proposed approach has been demonstrated with a dynamic simulation in an environment composed of two adjacent walls.

REFERENCES

[1] D. Hughes, "Uavs face hurdles in gaining access to civil airspace," *Aviation Week*, 2007.
[2] J. Roberts, P. Corke, and G. Buskey, "Low-cost flight control system for a small autonomous helicopter," in *2003 IEEE International Conference on Robotics and Automation*, vol. 1, pp. 546–551, 2003.
[3] P. Corke, "An inertial and visual sensing system for a small autonomous helicopter," *Journal of Robotic Systems*, vol. 21, no. 2, pp. 43–51, 2004.
[4] J. Lobo and J. Dias, "Vision and inertial sensor cooperation using gravity as a vertical reference," *IEEE Transactions on Pattern Analysis and Machine Intelligence*, vol. 25, no. 12, pp. 1597–1608, 2003.
[5] E. Altug, J. Ostrowski, and R. Mahony, "Control of a quadrotor helicopter using visual feedback," in *2002 IEEE International Conference on Robotics and Automation*, vol. 1, pp. 72–77, 2002.
[6] T. Hamel and R. Mahony, "Visual servoing of an under-actuated dynamic rigid-body system: an image-based approach," *IEEE Transactions on Robotics and Automation*, vol. 18, no. 2, pp. 187–198, 2002.
[7] R. Mahony, P. Corke, and T. Hamel, "Dynamic image-based visual servo control using centroid and optic flow features," *ASME Journal of Dynamic Systems, Measurement, and Control*, vol. 130, no. 1, p. 011005, 2008.
[8] J.-C. Zufferey and D. Floreano, "Fly-inspired visual steering of an ultralight indoor aircraft," *IEEE Transactions on Robotics*, vol. 22, no. 1, pp. 137–146, 2006.
[9] L. Muratet, S. Doncieux, Y. Briere, J. arcady Meyer A, and P. E. Blouin, "A contribution to vision-based autonomous helicopter flight in urban environments," *Robotics and Autonomous Systems*, vol. 50, pp. 195–209, 2005.
[10] F. Ruffier and N. Franceschini, "Visually guided micro-aerial vehicle: automatic take off, terrain following, landing and wind reaction," in *2004 IEEE International Conference on Robotics and Automation*, vol. 3, pp. 2339–2346, 2004.
[11] J. L. Barron, D. J. Fleet, and S. S. Beauchemin, "Performance of optical flow techniques," *International Journal of Computer Vision*, vol. 12, pp. 43–77, 1994.
[12] C. McCarthy, N. Barnes, and R. Mahony, "A robust docking strategy for a mobile robot using flow field divergence," *IEEE Transactions on Robotics*, vol. 24, no. 4, pp. 832–842, 2008.
[13] B. Hérissé, T. Hamel, R. Mahony, and F.-X. Russotto, "A terrain-following control approach for a VTOL unmanned aerial vehicle using average optical flow," *Autonomous Robots*, vol. 29, pp. 381–399, 2010.
[14] B. Hérissé, T. Hamel, R. Mahony, and F.-X. Russotto, "Landing a VTOL unmanned aerial vehicle on a moving platform using optical flow," *IEEE Transactions on Robotics*, vol. 28, no. 1, pp. 77–89, 2012.
[15] V. Lippiello, G. Loianno, and B. Siciliano, "MAV indoor navigation based on a closed-form solution for absolute scale velocity estimation using optical flow and inertial data," in *2011 50th IEEE Conference on Decision and Control and European Control Conference*, pp. 3566–3571, 2011.
[16] J. Stowers, M. Hayes, and A. Bainbridge-Smith, "Biologically inspired uav obstacle avoidance and control using monocular optical flow & divergence templates," in *2011 5th International Conference on Automation, Robotics and Applications*, pp. 378–383, 2011.
[17] M. Srinivasan, J. Chahl, K. Weber, S. Venkatesh, M. Nagle, and S. Zhang, "Robot navigation inspired by principles of insect vision," *Robotics and Autonomous Systems*, vol. 26, no. 23, pp. 203–216, 1999.
[18] L. Mejias, J. Correa, I. Mondragon, and P. Campoy, "Colibri: A vision-guided uav for surveillance and visual inspection," in *2007 IEEE International Conference on Robotics and Automation*, pp. 2760–2761, 2007.
[19] D. Jones, "Power line inspection — an UAV concept," in *The IEE Forum on Autonomous Systems*, 2005.
[20] F. Caballero, L. Merino, J. Ferruz, and A. Ollero, "A visual odometer without 3d reconstruction for aerial vehicles. applications to building inspection," in *2005 IEEE International Conference on Robotics and Automation*, pp. 4673–4678, 2005.
[21] L. Zou and Y. Li, "A method of stereo vision matching based on opencv," in *International Conference on Audio Language and Image Processing*, pp. 185–190, 2010.
[22] Q. Wang, H. Xu, S. Li, F. Yu, and S. Li, "Keypoint matching in stereo vision," in *International Conference on Information Science and Engineering*, pp. 6700–6703, 2010.
[23] M. Calonder, V. Lepetit, M. Ozuysal, T. Trzcinski, C. Strecha, and P. Fua, "Brief: Computing a local binary descriptor very fast," *IEEE Transactions on Pattern Analysis and Machine Intelligence*, vol. 34, no. 7, pp. 1281–1298, 2012.
[24] J. Liu and X. Liang, "I-brief: A fast feature point descriptor with more robust features," in *International Conference on Signal-Image Technology and Internet-Based Systems*, pp. 322–328, 2011.
[25] J. J. Koenderink and A. J. Doorn, "Facts on optic flow," *Biological Cybernetics*, vol. 56, pp. 247–254, 1987.
[26] N. Metni, J.-M. Pflimlin, T. Hamel, and P. Soueres, "Attitude and gyro bias estimation for a flying uav," in *2005 IEEE/RSJ International Conference on Intelligent Robots and Systems*, pp. 1114–1120, 2005.
[27] R. Mahony and T. Hamel, "Robust trajectory tracking for a scale model autonomous helicopter," *International Journal of Robust and Nonlinear Control*, vol. 14, pp. 1035–1059, 2004.
[28] H. Khalil, *Nonlinear Systems*. Pearson Education, 3th ed., 2000.